Chapter 4

2D-SnS_2 NANOFLAKES BASED EFFICIENT ULTRAVIOLET PHOTODETECTOR

This chapter reports the fabrication and characterization of a photoconductor structure (Ag/2D-SnS_2/Ag) based on one pot solvothermal synthesized SnS_2 nanoflakes materials. The introduction of a newly explored TMDs materials i.e., SnS_2 has been studied in this chapter to overcome the disadvantage of the low absorption of graphene for the broad light illumination as discussed in Chapter-3. The low absorption of graphene limits the performance of photodetection structure and also enhance the overall fabrication cost by involving CVD technique. The fabricated simplest and cost effective SnS_2 nanoflakes structure has been studied under broad light illumination. The realized structure shows efficient optical performance in UV regions while its start degrading in visible and NIR regions due to low absorption [*]

[*]Parts of this chapter have been published in Sanjeev Mani Yadav, and Amritanshu Pandey. "2D-SnS_2 Nanoflakes Based Efficient Ultraviolet Photodetector." *IEEE Transactions on Nanotechnology* 19 (2020): 301-307

4.1 Introduction

The high energy ultraviolet (UV) radiations in the environment affect almost all biological actions of living body in either way. It supports in synthesis of vitamin-D by skin in humans and helps in vision and navigation of animals and insects. However, it can cause damage to bio-molecules and immune system, sunburn the skin and cataracts human eyes. Different UV wavelengths and intensities are widely used in industrial and medical purposes such as disinfection, sterilization, and photo-therapy. Therefore, highly spectrum sensitive UV photodetectors with high signal-to-noise ratio, high responsivity, high detectivity and fast response time are required in wide variety of applications including UV photography, flame sensing, biological and medical treatment [272, 273, 274, 275, 276].

The UV photodetectors fabricated using popularly used wide bandgap semiconductors (ZnO, TiO_2, SnO_2 etc.) have unsatisfactory optical characteristics [277, 278, 279, 280]. Hence, costly, hybrid and complex photodetection structures are employed to enhance the performance of photodetectors. Some high mobility materials such as graphene is utilized to improve the time response/speed of the photodetectors. Further, some high surface to volume ratio structures such as nanorods, quantum dots (QDs), nanotube arrays etc., are employed to enhance the optical absorption thus, improving the performance of these devices in terms of responsivity, EQE and detectivity [281, 282, 283, 284, 285, 286].

2D materials have established an important place for their suitability as optoelectronic material owing to it excellent optical-electrical interaction properties over wide range of wavelengths. The devices based on 2D layered semiconductors have applications including photodetector, high speed transistors, flexible display, super capacitor, chemical/biological sensors, strain sensors, bioimaging, nanogenerators, and innovative nanoelectromechanical systems [287, 288]. Photodetectors based on nanostructures of large bandgap 2D materials may be a better choice in UV photodetection due to their intriguing properties which are different from those of their corresponding bulk state [51, 288, 289]. Various 2D materials (MoS_2, WS_2, $MoSe_2$ etc.) based photodetector

are reported in the literature [290, 291, 234], but due to their bandgap falling between 1 to 2 eV [292], the operation is limited to either in visible or in near infrared (NIR) region. The pursuit for 2D materials with larger band gap and high absorption coefficient in UV region is underway so that high responsivity, detectivity, and EQE of UV photodetectors may be achieved.

SnS_2, a nontoxic, environment-friendly, abundant, large bandgap, n-type 2D semiconductor material, belongs to CdI_2-type structure [236]. It has high absorption coefficient (10000 cm^{-1}) [293] and moderate carrier mobility (230 cm^2/V-s) [119]. SnS_2 materials have been widely used in the field of lithium-ion batteries, field effect transistor, solar cells and photocatalysis, in resent of years [237, 238, 294]. However, there are very few reports on SnS_2 based photodetectors which motivated us to explore it for UV photodetection. Due to its favourable properties SnS_2 can be used to get rid of the requirement of additional materials such as QDs, nanorods etc., resulting in simple yet efficient photodetector structure. Moreover, the bandgap of nanoparticles are size dependent and therefore bandgap tunability [295] may be achieved by the use of various size of SnS_2 nanostructures. The one-step solvothermal synthesis of SnS_2 nanoflakes leads to low-cost SnS_2 based UV detector.

This chapter reports solvothermal synthesis of SnS_2 nanoflakes for UV photodetection applications. The SnS_2 nanoflakes are spin coated over silicon substrate to produce resultant SnS_2 nanoflakes/SiO_2/Si based UV photodetectors. The structural and optical characterizations have been performed for the confirmation of SnS_2 crystalline phase and their optical bandgap, respectively. The optoelectronic characterizations of SnS_2 nanoflakes/SiO_2/Si UV photodetectors have been performed by I-V characteristics, responsivity, detectivity, and time response measurements. Furthermore, the thermal stability analysis of the device was also performed by measuring I-V characteristics for large temperature variation. Hence, highly sensitive, temperature stable, and cost-effective 2D-SnS_2 nanoflakes based UV Photodetectors have been realized.

4.2 Experimental Details

4.2.1 Solvothermal Synthesis of SnS_2 Nanoflakes

The solvothermal synthesis of SnS_2 nanoflakes were performed by dissolving 1 mmol of $SnCl_4.5H_2O$ and 2.5 mmol of Thiourea in 30 ml Ethylene glycol using magnetic stirring followed by ultrasound treatment to form a transparent solution as per literature [239]. The resultant transparent solution was transferred in 50 ml Teflon-lined autoclave and was placed in an oven at 180^{o}C for ∼24 h. After cooling the resultant solution, at room temperature SnS_2 nanoflakes in form of yellow precipitates were collected. The schematic of solvothermal synthesis of SnS_2 Nanoflakes is shown in Fig.4.1

Figure 4.1: Solvothermal synthesis of SnS_2 nanoflakes

4.2.2 Device Fabrication

The device fabrication starts by considering a p-silicon substrate of size ∼(1×1 cm^2, Area) with a resistivity of 2-7 ohm-cm. The cleaned substrate was oxidized in a high-temperature furnace to achieve a 300 nm SiO_2 layer over it. In the next step, the synthesized SnS_2 nanoflakes were spin coated over SiO_2/Si substrate at 2500 r.p.m. for 30 sec and then the resultant device was heated on a hot plate for 3 min at 130^{o}C. The above process is repeated for four times to achieve uniform and continuous coating of SnS_2 nanoflakes over SiO_2/Si substrate. In the final step, Ag electrodes of diameter

2 mm and thickness ∼50 nm were patterned on SnS_2 nanoflakes/SiO_2/Si structure by using shadow masking in thermal coating unit. The schematic and pictorial top view of the resultant fabricated devices are shown in Fig.4.2 (a) and (b), respectively. The atomic arrangement of SnS_2 in form of 2D structure is also depicted in Fig.4.2 (c).

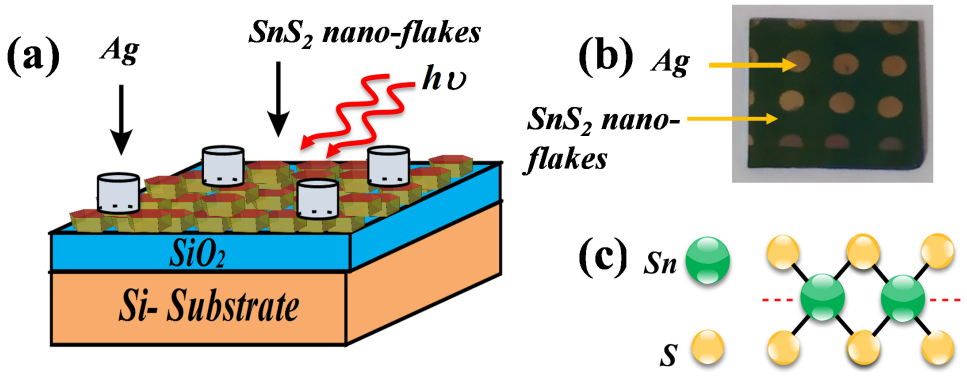

Figure 4.2: (a) The device schematic of Ag/SnS_2 nanoflakes/SiO_2/Si photodetector, (b) Fabricated device under consideration, and (c) Atomic arrangement 2D-SnS_2.

4.3 Results and Discussion

4.3.1 Structural and Optical Characterization

The X-ray diffraction (X-RD) analysis of solvothermal synthesized SnS_2 nanoflakes performed by Rigaku smart-lab 9 kW equipped with a Cu K-α source of 1.5405 Å wavelength is shown in Fig.4.3 (a). The X-RD pattern with high intense and narrow peak confirms the high crystalline plane orientation for (001) and (101) plane indexing. The X-RD pattern of SnS_2 also confirms the crystal structure of the hexagonal phase matched well with the JCPDS 023-0677 data. The Raman analysis of SnS_2 nanoflakes was recorded using Raman Spectrophotometer (Renishaw inVia, Germany) with laser excitation of 532 nm. In Raman spectra (Fig.4.3 (b)) the peak observed at 312.42 cm^{-1} corresponds to the A_{1g} modes of 2H-SnS_2 [296]. The absorption spectra (Fig.4.3 (c)) of synthesized SnS_2 nanoflakes was performed by PerkinElmer, Lambda 25-UV/Vis Spectrometer. Fig.4.3 (c) confirms the high absorption in UV region by SnS_2 nanoflakes. Thus, the potentiality of synthesized SnS_2 nanoflakes for UV detection is expected.

From the Tauc-plot (Inset in Fig.4.3 (c)) it is derived that synthesized SnS_2 nanoflakes possess direct transition with multiple band gaps of 3.29, 4.17 and 5.27 eV. The photo-luminescence (PL) analysis of SnS_2 was performed by LS-45 Fluorescence Spectrometer, PerkinElmer at various excitation wavelengths (Fig.4.3 (d)). The strong emission peak is observed at ∼385 nm irrespective of excitation wavelengths, corresponding to band gap of ∼3.22 eV which is matched well with the band gap calculated from Tauc-plot i.e.,∼3.29 eV. In addition, the single emission peak obtained in PL spectra is attributed to the direct transitions of the carriers at ∼3.22 eV. While the emission peaks regarding sub-band (shown in Fig.4.3 (c)) transition which occurs due to the presence of interface or interior defects in the material are reasonably very weak hence are not observed in PL spectra [117].

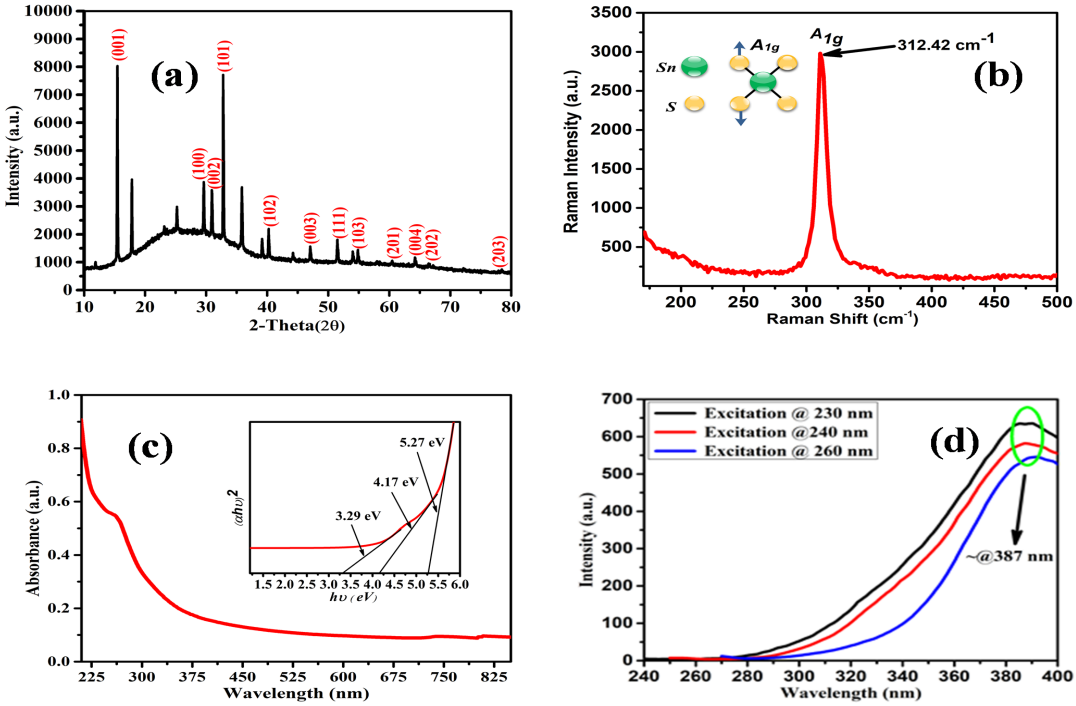

Figure 4.3: (a) X-RD pattern of solvothermal synthesized SnS_2 nanoflakes, (b) Raman spectra of SnS_2 nanoflakes with A_{1g} mode, (c) Absorption spectra of SnS_2 with Tauc-plot inset, (d) PL spectra of solvothermal synthesized SnS_2 nanoflakes with three excitation wavelengths i.e 230, 240, and 260 nm with constant emission peak at ∼387 nm.

The Transmission electron microscopy (TEM), high-resolution TEM (HR-TEM), and selected area electron diffraction (SAED) pattern analysis of solvothermal syn-

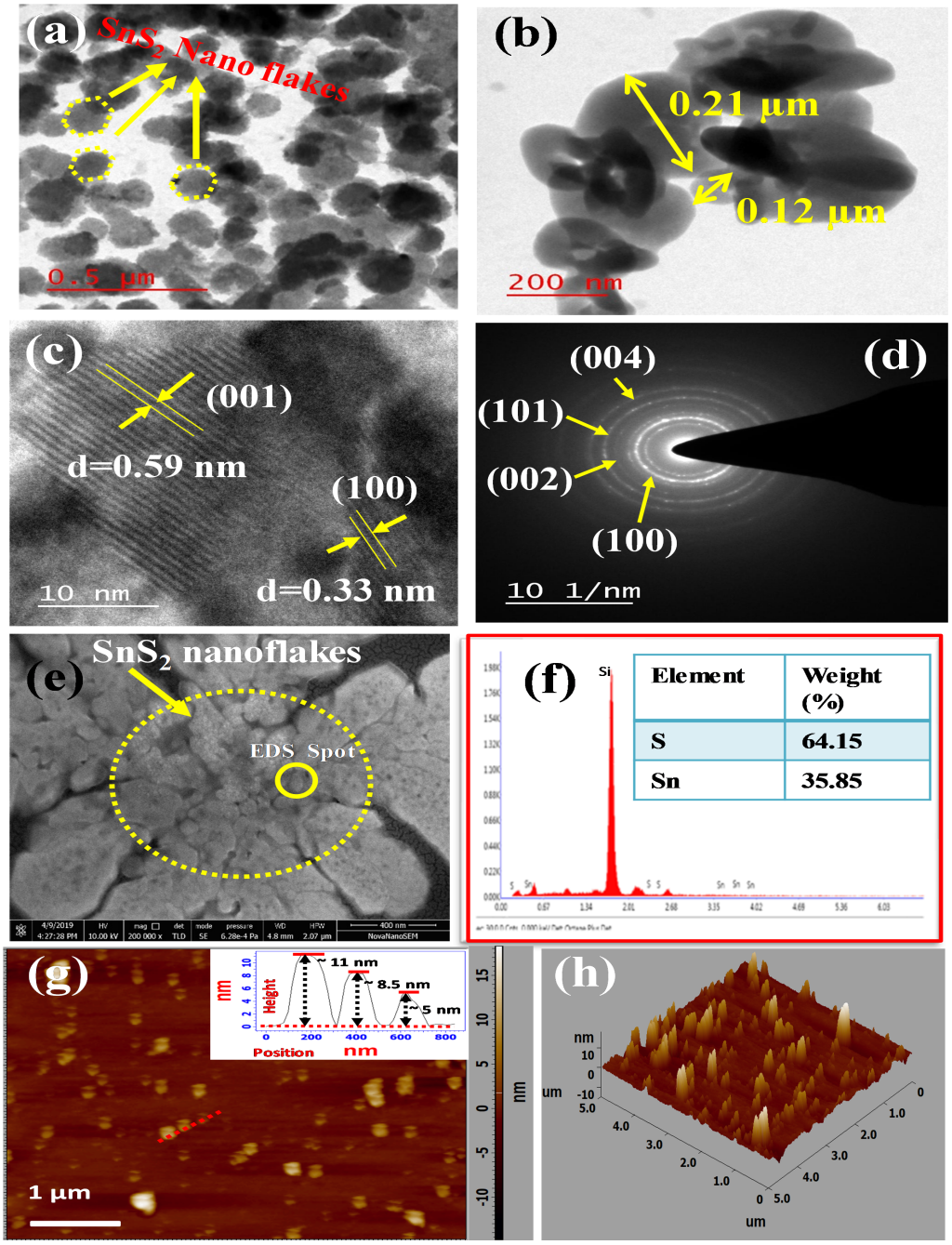

Figure 4.4: (a) TEM micrographs showing high resolution hexagonal shaped SnS_2 nanoflakes, (b) TEM image of SnS_2 nanoflakes with marked dimensions at 200 nm scale, (c) HR-TEM image of SnS_2 nanoflakes with inter planar spacing, (d) SAED pattern of SnS_2 nanoflakes with plane indexing, (e) FE-SEM image of SnS_2 over SiO_2/Si substrate, (f) EDS spectra for selected spot in Fig.4.4 (e) with element Sn, S and their elemental weight(%), (g) AFM image of SnS_2 nanoflakes over SiO_2/Si substrate with height profile (Inset), (h) 3D profile of SnS_2 nanoflakes over SiO_2/Si for corresponding AFM image in Fig.4.4 (g)

thesized SnS_2 nanoflakes were performed by using Tecnai G2 20 Twin of FEI, USA. The TEM image (Fig.4.4 (a)) confirms the almost hexagonal shaped morphology of SnS_2 nanoflakes. The TEM image of SnS_2 nanoflakes with marked dimensions 0.21 μm and 0.12 μm oriented in various directions with estimated average flakes dimension of $\sim$0.16 μm is shown in Fig.4.4 (b). Fig.4.4 (c) shows the HR-TEM image of SnS_2 nanoflakes with inter planar spacing and its corresponding plan indexing. SAED pattern of solvothermal synthesized SnS_2 nanoflakes with bright and circular rings are shown in Fig.4.4 (d). The clear and bright circular rings along with marked planes observed in the diffraction pattern confirm the highly crystalline hexagonal phase geometry of SnS_2 nanoflakes. To understand the shape and surface morphology of SnS_2 nanoflakes over SiO_2/Si substrate the Field Emission Scanning Electron Microscopy (FE-SEM) analysis have been performed by Nova Nano SEM 450 of FEI, USA. The FE-SEM image of SnS_2 nanoflakes confirms the presence of highly dense and overlapped nanoflakes over SiO_2/Si as shown in Fig.4.4 (e). Further to know the presence of various elements and their composition the Energy-dispersive X-ray spectroscopy (EDS) analysis of the selected portion in FE-SEM image has been performed (Fig.4.4 (f)). The obtained EDS data for selected spot confirm the presence of Sn and S element and also provide its elemental weight (%). Atomic force morphology (AFM) performed using NTEGRA Prima, NT-MDT Service & Logistics Ltd. of mono layer SnS_2 nanoflakes spin coated over SiO_2/Si substrate is shown in Fig.4.4 (g). The nanoflakes of height $\sim$5, $\sim$8.5 and $\sim$11 nm have been observed for the selected portion in AFM image thus validates the nanoflakes/nanosheets geometry of synthesized SnS_2[239, 297]. Further the 3D profile of SnS_2 nanoflakes for corresponding AFM image has been recorded (Fig.4.4 (h)).

4.3.2 Electrical Characterization

The current-voltage characterization of a fabricated photoconductive type [298, 299, 300, 301, 302, 303] device has been performed with the help of a parameter analyzer (Keysight, B1500A) and a UV light source. The source has center frequency at $\sim$365 nm and optical power density $\sim$1.112 mW/cm^2. The current–voltage (I–V) plot of fabricated Ag/SnS_2 nanoflakes/SiO_2/Si photodetector is shown in Fig.4.5 (a). The I–V

plot of the device suggests the existence of ohmic contact between Ag and SnS_2. This is in confirmation with theoretical prediction of ohmic contact between n-SnS_2 and Ag, since the work function of SnS_2 (∼5.1 eV) is larger than the work function of Ag (∼4.2 eV) [244, 304]. The contrast ratio, defined as ratio of UV illuminated current and dark current, of the fabricated SnS_2 nanoflakes based device is shown in Fig.4.5 (b) for different bias. The fabricated device has large and approximately constant contrast ratio (sensitivity) even at low external bias. The observed contrast ratio (∼400) is significantly larger in comparison to the reported UV photodetectors [245, 246, 247] hence; the fabricated device can work at lower voltage without degrading its performance in terms of its photodetection characteristic. The fabricated photodetector has applications in UV curing, counterfeit detection, air purification, and ozone sensing [305] etc., where high intensity (>1 mW/cm^2) UV radiations are employed.

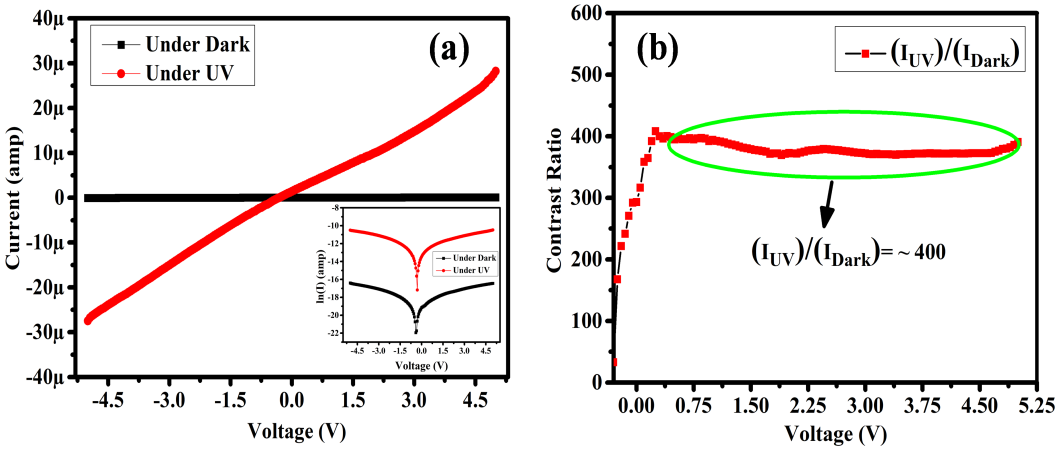

Figure 4.5: (a) I–V characteristics of fabricated Ag/SnS_2 nanoflakes/SiO_2/Si photodetector with an alternate ln(I)–V plot (Inset), (b) Contrast ratio of the photodetector under UV light (∼365 nm) illumination

The band diagram along with carrier transport mechanism for Ag/n-SnS_2/Ag photoconductor is presented in Fig.4.6, here the work function of the Ag and SnS_2 nanoflakes are given by ϕ_{Ag} and ϕ_{SnS2} respectively. Whereas, E_F, E_C, and E_V are Fermi, conduction and valence band energy levels. The electron affinity of n-SnS_2 nanoflakes is represented by χ_{SnS2}. Ohmic contact is observed between Ag and SnS_2. Thus, the unopposed movement of photo-generated carriers in SnS_2 nanoflakes leads the linear relationship of current with applied positive and negative bias voltages. The large photo

currents have been observed due to high absorption coefficient (10000 cm^{-1}) [293] of SnS_2 nanoflakes under UV illumination.

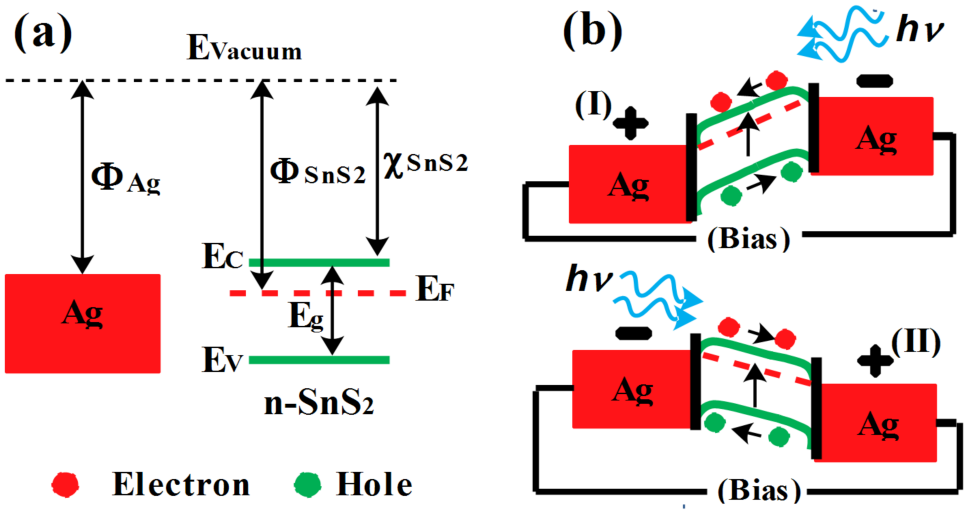

Figure 4.6: (a) Band energy diagram of Ag and n-type SnS_2 nanoflakes before contact, (b) After contact at thermal equilibrium with UV light illumination; For case-(I) left side Ag electrode at positive voltage, and for case-(II) right side Ag electrode at positive voltage.

The temperature-based analysis of SnS_2 nanoflakes photodetector have been performed under a special setup capable of varying temperature of the device. The resultant current-voltage characteristics, measured from 60^{o}C to 120^{o}C in step of 10^{o}C, have been shown in Fig.4.7. It is evident that with rise in temperature very small change in current is observed at a particular fixed bias. For example, the increase in the current at 5 V bias for 60^{o}C to 120^{o}C increase in temperature has been found to be only ~2 times. The results suggest that the optical characteristics (i.e., Responsivity, Detectivity, EQE etc.) stability of our photodetector is better than the reported UV photodetectors [253, 306]. The high-thermal stability of this device makes it a suitable candidate for the detection of UV irradiation with high accuracy and stability; and can be used in applications such as coal mining, remote sensing, and bio-imaging etc. [305]

Further, the spectral analysis of the photodetector was performed with the help of a monochromator (Princeton Instruments, SP2150i), a light source and a digital multimeter (Agilent, 34410A) with wavelength scan rate 60 nm/min. The light source of variable optical power density was used to illuminate the fabricated photodetector. The

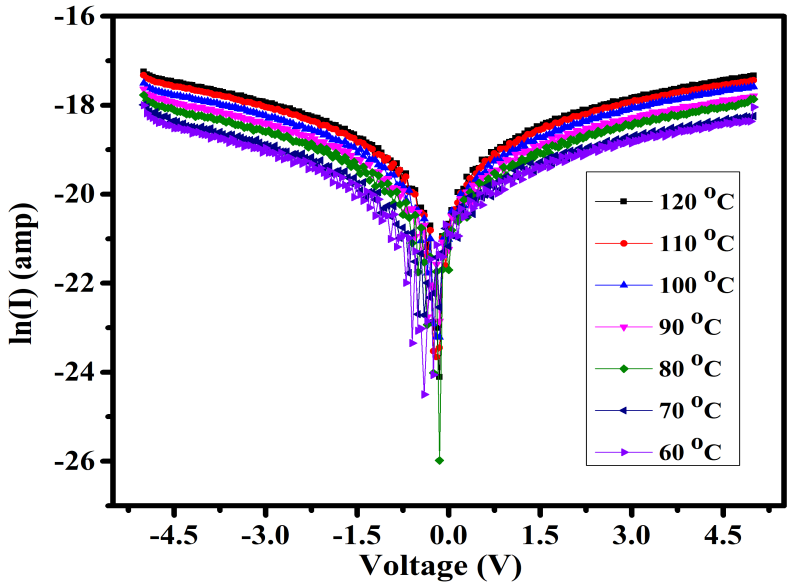

Figure 4.7: ln (I)–V characteristics of Ag/SnS_2 nanoflakes/SiO_2/Si photodetector at various temperature.

observed high current density for UV range (Fig.4.8 (a)) suggests that the fabricated SnS_2 nanoflakes based photodetector has promising characteristics in this region.

The figure-of-merit of SnS_2 nanoflakes based photodetector such as responsivity (R), EQE and detectivity (D) are measured by using equations (4.1)-(4.3) and are presented in Fig.4.8.

$$Responsivity(R) = \frac{I_p}{P_{opt}.S} \tag{4.1}$$

where I_P is the photocurrent at an applied bias when illuminated with an optical power density of P_{opt} and S is the effective illumination area ($\sim$0.038 cm^2) of the device.

The calculation of EQE, a measure of optical to electrical conversion efficiency of the detector, is done by the following relation [248]

$$EQE(\eta) = \frac{hc}{\lambda q}R = \sim \frac{1240}{\lambda(nm)}R \tag{4.2}$$

The voltage-dependent detectivity (D) of the device can be define as [307].

$$Detectivity(D) = \frac{\lambda\eta q}{hc}\sqrt{\frac{RA}{4kT}} \tag{4.3}$$

In equation 4.3 the ratio q$\eta\lambda$/hc denotes the responsivity (R) of the device in term of external quantum efficiency (η), illuminated light wavelength (λ), electronic charge (q=1.6×10^{-19} C), Planck's constant (h = 6.63×10^{-34} $m^2kg.s^{-1}$) and (c= 3×10^8 $m.s^{-1}$). In addition, in (4), (k =1.38×10^{-23} $m^2kg.s^{-2}K^{-1}$) is Boltzmann constant, T (300 K) is room temperature. (RA) is the resistance area product and defined as,

$$\left(\frac{\partial J}{\partial V}\right)^{-1} = \frac{kT}{qJ} = RA \tag{4.4}$$

The responsivity, EQE(%) and detectivity of the fabricated device have been found to be ∼5.5 A/W, ∼1868% and ∼1.72×10^{13} Jones (1 Jones = 1 cm $Hz^{1/2}W^{-1}$), respectively for ∼365 nm wavelength illumination and 5 V applied bias. As observed from Fig.4.8, better responsivity, detectivity and EQE (%) of the device have been achieved at lower wavelength of UV radiation (< 365 nm). For illustration, responsivity, detectivity and EQE(%) at ∼315 nm are found to be ∼10 A/W, ∼3.23×10^{13} Jones and ∼3936%, respectively.

The fabricated device shows the sufficient high responsivity, EQE(%) and detectivity for ∼315 nm illumination wavelength for low illumination power density and confirm its potentiality for UV photodetection. Although, the optical parameters i.e., R, EQE(%) and D of the device for 400-600 nm (visible) illumination wavelengths have been also obtained, the obtained parameters have been observed to be sufficiently smaller than the parameters observed for ∼315 nm UV illumination. Therefore, this structure is a efficient UV photodetector and has superior characteristics compared with previously reported results.[308, 309]

The time response (Fig.4.8 (d)) of the device has been measured under a UV source of central frequency ∼365 nm at 5 V bias with optical power density ∼1.112 mW/cm^2 (measured by Thorlabs PM100D power meter). The ON and OFF time of the source kept 20 s in each cycle. The rise time (10%-90%) and fall time (90%-10%) of device were recorded and found to be 2.2 and 6.3 s respectively. The slow rise time of the

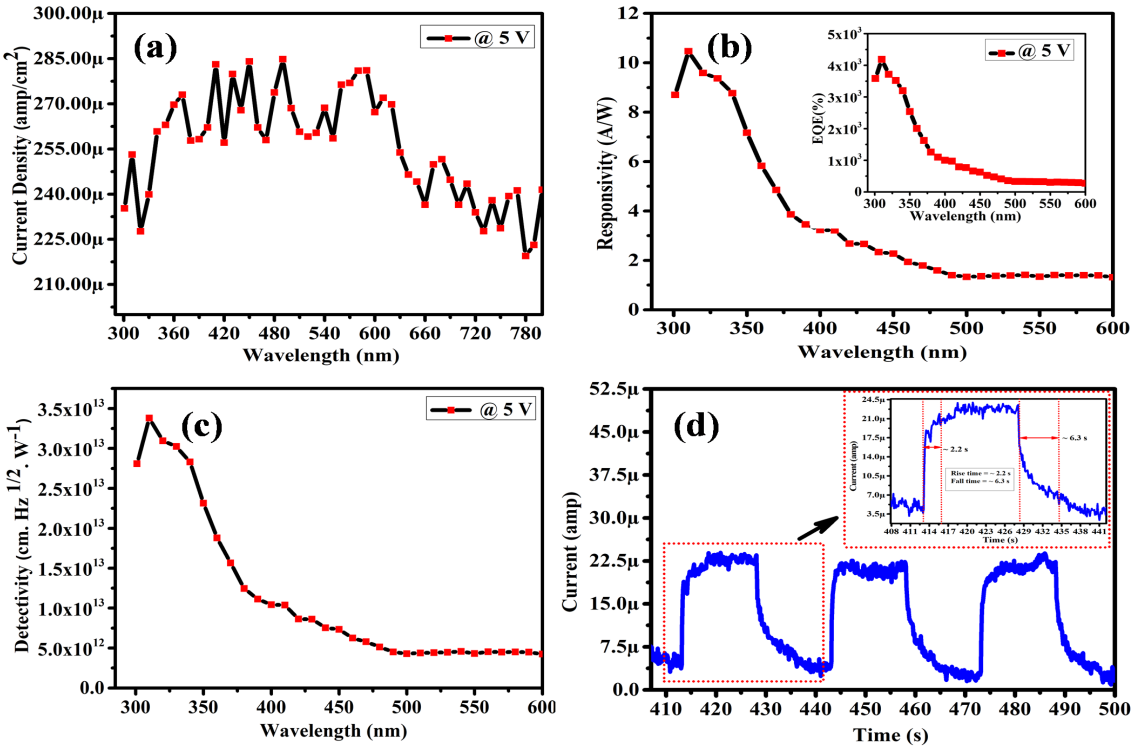

Figure 4.8: (a) Current density, (b) Responsivity (Inset EQE (%)), (c) Detectivity of device as function of wavelength, and (d) Time response of device at ∼365 nm wavelength with optical power density ∼1.112 mW/cm^2

fabricated photodetector is mainly attributed to the large channel spacing between two Ag electrodes which results in increase in the time taken by the photo-generated charge carriers to reach the electrodes. Hence, the time response of the fabricated detector can be improved by reducing the separation between two electrodes [303].

The large responsivity, detectivity and better time response of our fabricated device compared to other reports [245, 247, 310, 280, 251, 246, 252] make it better choice for UV photodetection. To point out the significance, a comparison of our fabricated SnS_2 nanoflakes based photodetector with some other UV photodetectors is presented in Table-4.1.

4.4 Conclusion

In this chapter, we have reported the fabrication and characterization of a newly explored TMDs named as SnS_2 for efficient UV photodetection. The SnS_2 nanoflakes have

Table 4.1: Comparison With Some Other Reported UV-Photodetectors

Parameters	**This work**	**[310]**	**[245]**	**[246]**	**[247]**	**[280]**
Device structure	Ag/SnS_2 nanoflakes	SnS_2/PP-substrate	Au/ZnO seed layer	Ag/ZnO QDs	TiO_2/Water -solid substrate	SnO_2 based
Applied Bias (V)	5	5	1	2	(-1 to +1)	5
Wavelength (nm)	365	365	360, 365	360	365	340
Illumination Intensity (mW/cm^2)	0.05074	3.87 μW	0.496	0.070	(0.113—2.44)	—-
Contrast -Ratio (I_{light}/I_{dark})	400 @(0.25—5V)	—	137	∼50 @(2–5V)	(2–6)	—-
Responsivity (A/W)	5.5	2.06× 10^{-4}	0.0544	15.04	0.06	18× 10^{-6}
Detectivity (Jones)	∼1.72×10^{13}	—-	—-	1.97×10^{14}	—-	—-
EQE (%)	1868	—-	—-	—-	—-	—-
Time Response (ON and OFF)	2.2 and 6.3 s (@ 365 nm)	—-	8.67 and 5.39 s	7.2 and 18.5 s (@ 390 nm)	0.5 and 0.5 s	—-

been synthesized by using simplest solvothermal technique. SnS_2 material has been explored in this chapter to overcome the limitations of graphene. The fabricated SnS_2 nanoflakes/SiO_2/Si photodetector offers high contrast ratio (∼400), high responsivity (∼5.5 A/W) and detectivity (∼1.72×10^{13} Jones) under UV light illumination. The temperature based ln(I)-V characteristics analysis of photodetector was also performed for the range of 60^{o}C to 120^{o}C to confirm the thermal stability of the device. Furthermore, the response time of our fabricated device under UV irradiation was found to be around ∼2.2 s. The large responsivity, detectivity and good time response of our fabricated device make it better choice for UV photodetection. The fabricated UV detector may have variety of applications in health monitoring, bio-sensing, UV spectroscopy, and flame detection etc., due to it's simple, and cost-effective fabrication.